Therapeutic targeting of HER2–CB_2R heteromers in HER2-positive breast cancer

Sandra Blasco-Benito[a,b], Estefanía Moreno[c,d,e], Marta Seijo-Vila[a,b], Isabel Tundidor[a,b], Clara Andradas[a,1], María M. Caffarel[f,g], Miriam Caro-Villalobos[a,b], Leyre Urigüen[h,i], Rebeca Diez-Alarcia[h,i], Gema Moreno-Bueno[j,k,l,m,n], Lucía Hernández[b,o], Luis Manso[b,p], Patricia Homar-Ruano[c,d,e], Peter J. McCormick[q,2], Lucka Bibic[q], Cristina Bernadó-Morales[n,r], Joaquín Arribas[n,r,s], Meritxell Canals[t], Vicent Casadó[c,d,e], Enric I. Canela[c,d,e], Manuel Guzmán[a,e,u], Eduardo Pérez-Gómez[a,b,3], and Cristina Sánchez[a,b,3]

[a]Department of Biochemistry and Molecular Biology, Complutense University, 28040 Madrid, Spain; [b]Instituto de Investigación Hospital 12 de Octubre, 28041 Madrid, Spain; [c]Department of Biochemistry and Molecular Biomedicine, University of Barcelona, 08028 Barcelona, Spain; [d]Institute of Biomedicine, University of Barcelona, 08028 Barcelona, Spain; [e]Centro de Investigación Biomédica en Red de Enfermedades Neurodegenerativas (CIBERNED), 28031 Madrid, Spain; [f]Basque Foundation for Science (IKERBASQUE), 48013 Bilbao, Spain; [g]Molecular Oncology Group, Biodonostia Health Research Institute, 20014 San Sebastian, Spain; [h]Department of Pharmacology, University of the Basque Country Universidad del País Vasco/Euskal Herriko Unibersitatea, 48940 Leioa, Spain; [i]Centro de Investigación Biomédica en Red de Salud Mental (CIBERSAM), 28029 Madrid, Spain; [j]Department of Biochemistry, Universidad Autónoma de Madrid (UAM), 28049 Madrid, Spain; [k]Instituto de Investigaciones Biomédicas "Alberto Sols," Consejo Superior de Investigaciones Científicas-UAM, 28029 Madrid, Spain; [l]Instituto de Investigación Hospital Universitario La Paz (IdiPAZ), 28046 Madrid, Spain; [m]Fundación MD Anderson Internacional, 28033 Madrid, Spain; [n]Centro de Investigación Biomédica en Red de Cáncer (CIBERONC), 28029 Madrid, Spain; [o]Pathology Unit, Hospital 12 de Octubre, 28041 Madrid, Spain; [p]Medical Oncology Department, Hospital 12 de Octubre, 28041 Madrid, Spain; [q]School of Pharmacy, University of East Anglia, Norwich, Norfolk NR4 7TJ, United Kingdom; [r]Preclinical Research Program, Vall d'Hebron Institute of Oncology, 08035 Barcelona, Spain; [s]Department of Biochemistry and Molecular Biology, Institució Catalana de Recerca i Estudis Avançats, Universitat Autónoma de Barcelona, 08193 Barcelona, Spain; [t]Monash Institute of Pharmaceutical Sciences, Monash University, Parkville, VIC 3052, Australia; and [u]Instituto Ramón y Cajal de Investigación Sanitaria, 28034 Madrid, Spain

Edited by William J. Muller, McGill University, Montreal, QC, Canada, and accepted by Editorial Board Member Peter K. Vogt January 3, 2019 (received for review September 3, 2018)

Although human epidermal growth factor receptor 2 (HER2)-targeted therapies have dramatically improved the clinical outcome of HER2-positive breast cancer patients, innate and acquired resistance remains an important clinical challenge. New therapeutic approaches and diagnostic tools for identification, stratification, and treatment of patients at higher risk of resistance and recurrence are therefore warranted. Here, we unveil a mechanism controlling the oncogenic activity of HER2: heteromerization with the cannabinoid receptor CB_2R. We show that HER2 physically interacts with CB_2R in breast cancer cells, and that the expression of these heteromers correlates with poor patient prognosis. The cannabinoid Δ^9-tetrahydrocannabinol (THC) disrupts HER2–CB_2R complexes by selectively binding to CB_2R, which leads to (*i*) the inactivation of HER2 through disruption of HER2–HER2 homodimers, and (*ii*) the subsequent degradation of HER2 by the proteasome via the E3 ligase c-CBL. This in turn triggers antitumor responses in vitro and in vivo. Selective targeting of CB_2R transmembrane region 5 mimicked THC effects. Together, these findings define HER2–CB_2R heteromers as new potential targets for antitumor therapies and biomarkers with prognostic value in HER2-positive breast cancer.

breast cancer | HER2 | cannabinoids | receptor heteromers | CB_2R

Breast cancer is a very heterogeneous disease in terms of molecular markers, prognosis, and treatments. According to all subclassification methods, there is a specific subtype that is characterized by overexpression of human epidermal growth factor receptor 2 (HER2), which represents roughly 15 to 20% of all breast tumors (1, 2). HER2 belongs to the ERBB (HER) receptor tyrosine kinase family, which consists of four members: HER1 (epidermal growth factor receptor; EGFR), HER2, HER3, and HER4. HER2 promotes oncogenic signaling by modulating the expression and activity of proteins controlling cell proliferation, differentiation, death, migration, and angiogenesis. Activation of HER2 is achieved by ligand- or overexpression-induced dimerization with other members of the family, followed by *trans*-phosphorylation and autophosphorylation of the two constituents of the HER homo/heterodimer in their cytosolic kinase domains (3, 4). Overexpression of HER2 in some ways is a paradigm for the design of targeted therapies for the management of this subtype of tumors. Thus, trastuzumab, a recombinant humanized monoclonal anti-HER2 antibody, has significantly improved the outcome of these patients (1, 4, 5). Despite its efficacy in many HER2+ breast cancer cases, some patients do not respond to this treatment and others eventually progress. Identifying the molecular mechanisms underlying HER2 activation (i.e., dimerization, *trans*- and autophosphorylation) has allowed the design of additional tools to overcome resistance to trastuzumab and

Significance

There is a subtype of breast cancer characterized by the overexpression of the oncogene HER2. Although most patients with this diagnosis benefit from HER2-targeted treatments, some do not respond to these therapies and others develop resistance with time. New tools are therefore warranted for the treatment of this patient population, and for early identification of those individuals at a higher risk of developing innate or acquired resistance to current treatments. Here, we show that HER2 forms heteromer complexes with the cannabinoid receptor CB_2R, the expression of these structures correlates with poor patient prognosis, and their disruption promotes antitumor responses. Collectively, our results support HER2–CB_2R heteromers as new therapeutic targets and prognostic tools in HER2+ breast cancer.

Author contributions: M.G., E.P.-G., and C.S. designed research; S.B.-B., E.M., M.S.-V., I.T., C.A., M.M.C., M.C.-V., L.U., R.D.-A., L.H., L.M., P.H.-R., P.J.M., L.B., M.C., and E.P.-G. performed research; G.M.-B., C.B.-M., and J.A. contributed new reagents/analytic tools; V.C., E.I.C., and C.S. analyzed data; and S.B.-B. and C.S. wrote the paper.

Conflict of interest statement: M.G. and C.S. are members of the Zelda Therapeutics Medical Advisory Board.

This article is a PNAS Direct Submission. W.J.M. is a guest editor invited by the Editorial Board.

[1]Present address: Area of Chronic and Severe Diseases, Telethon Kids Institute, Nedlands, WA 6009, Australia.

[2]Present address: Centre for Endocrinology, William Harvey Research Institute, Barts and The London School of Medicine and Dentistry, Queen Mary University of London, London EC1M 6BQ, United Kingdom.

[3]To whom correspondence may be addressed. Email: cristina.sanchez@quim.ucm.es or eduperez@ucm.es.

This article contains supporting information online at www.pnas.org/lookup/suppl/doi:10.1073/pnas.1815034116/-/DCSupplemental.

Published online February 7, 2019.

improve the treatment of these tumors. For example, pertuzumab, another anti-HER2 monoclonal antibody, was designed to specifically target the dimerization domain of HER2, and lapatinib, a tyrosine kinase inhibitor, to selectively inhibit the *trans*- and autophosphorylation of HER1 and HER2 (1, 4, 5). Simultaneous targeting of HER2 at different levels (i.e., combination of the aforementioned agents) is showing better clinical outcomes than anti-HER2 monotherapies, but some patients still present with either innate or acquired resistance (1, 5). Therefore, new/complementary therapeutic approaches are urgently needed to both identify and treat this patient population.

Cannabinoids, the active constituents of cannabis, produce antitumor responses in preclinical models of cancer, including HER2+ breast cancer (6–9). In most cases, the antitumor responses are produced by binding and activating cannabinoid receptors. CB_1R and CB_2R, the two cannabinoid receptors described so far, belong to the G protein-coupled receptor (GPCR) superfamily of membrane proteins. While CB_1R, the main receptor responsible for the psychoactive effects of cannabis, is widely expressed throughout the body and especially abundant in the central nervous system, CB_2R, in healthy individuals, is mainly restricted to elements of the immune system. However, increasing evidence shows that the expression of this receptor is augmented in many pathological states, including cancer (6–8). In fact, the preclinical research conducted so far in preclinical models of HER2+ breast cancer points to CB_2R as the main target of cannabinoid antitumor action (10, 11).

Here, we aimed at getting a deeper insight into the mechanisms of HER2 activation/inactivation, to provide new potential targets for treatment of HER2+ tumors. Specifically, we studied the functional relevance of a recently described heteromer between HER2 and the cannabinoid receptor CB_2. We have previously reported the presence of these complexes in HER2+ breast cancer tumors (12), but their role in HER2 function is as yet unknown. In this context, the main goal of this study was to determine the role of HER2–CB_2R heteromers in HER2+ breast cancer pathology and, overall, whether these structures could be new targets for anticancer treatments.

Results

HER2–CB_2R Heteromer Expression Correlates with Poor Patient Prognosis. We have previously described that CB_2R promotes HER2 prooncogenic signaling, and that these two membrane receptors physically interact in HER2+ breast cancer cells and tissue (12). However, the functional relevance of these heteromers is completely unknown. To evaluate their role in breast cancer, we first analyzed the expression of these complexes in a series of 57 human HER2+ breast cancer biopsies obtained at the time of first diagnosis, before any treatment [tissue microarray (TMA) 1 in *Materials and Methods*]. Proximity ligation assays (PLAs) (Fig. 1*A*) showed that higher HER2–CB_2R expression in tumors is associated with lower disease-free patient survival (Fig. 1*B*), as well as with higher spread to regional lymph nodes and Ki67 overexpression (*SI Appendix*, Table S1). To further validate these observations, we performed similar analyses in

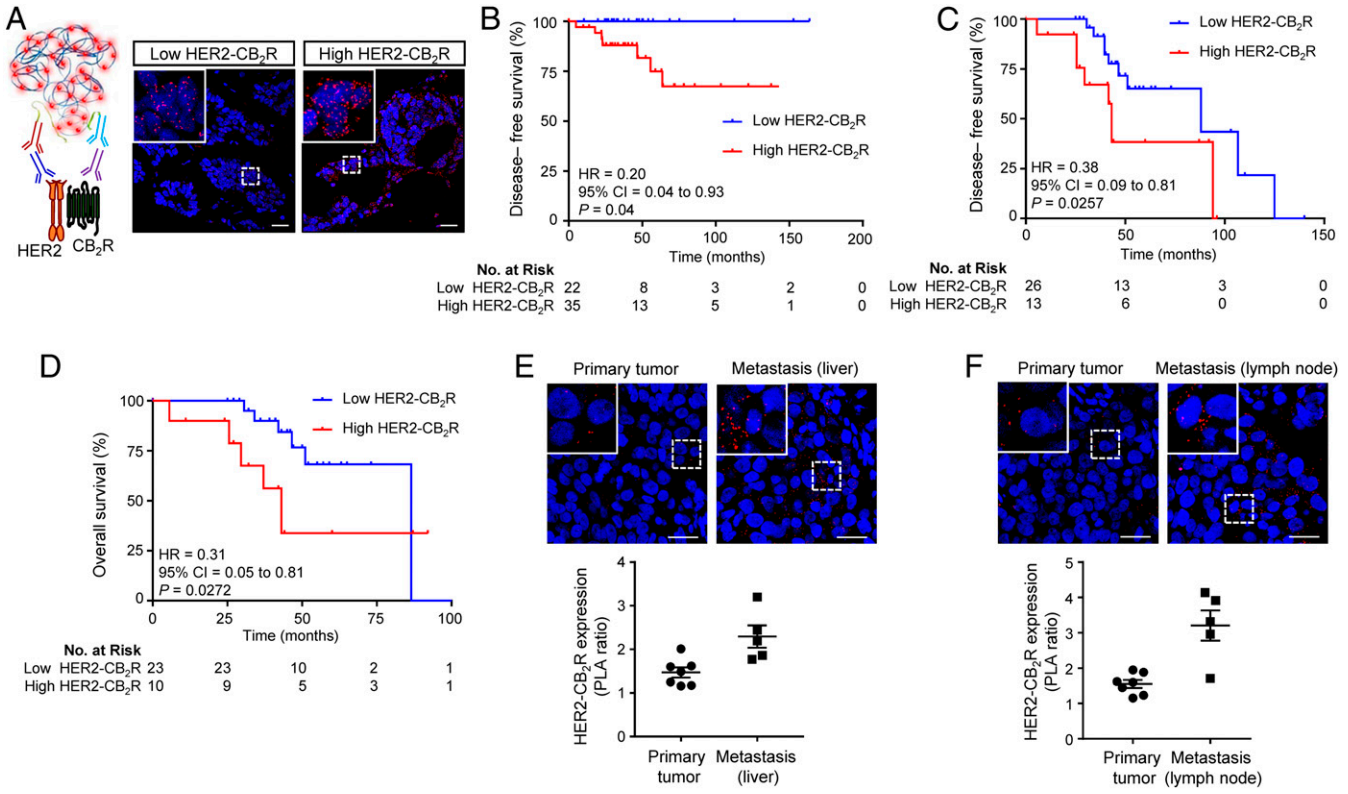

Fig. 1. HER2–CB_2R heteromer expression correlates with poor patient prognosis. Proximity ligation assays were performed in tissue microarrays and patient-derived xenografts. (Scale bars, 25 μm.) For the TMAs, samples were ranked based on HER2–CB_2R heteromer expression (i.e., PLA signal), and the best cutoff was manually selected. (*A*) Representative confocal microscopy images of a low– and a high–heteromer-expressing sample in TMA 1. The red dotted signal corresponds to the heteromers, and the blue staining corresponds to cell nuclei. (*B–D*) Kaplan–Meier curves for disease-free survival [from samples included in TMA 1 ($n = 57$) (*B*) or TMA 2 ($n = 39$) (*C*)] and overall patient survival [from the HER2+ samples included in TMA 2 ($n = 33$) (*D*)]. Curves were statistically compared by the log-rank test ($P < 0.05$). (*E* and *F*, *Upper*) Representative images of HER2–CB_2R heteromer expression in two pairs of PDXs, consisting of a PDX established from the patient's primary tumor and a sample derived from a metastasis in the same patient [in the liver in one case (*E*), and in a lymph node in the other (*F*)]. (*E* and *F*, *Lower*) Quantification of HER2–CB_2R heteromer expression in the PDX samples. Results are expressed as PLA ratio (number of red dots per cell), and error bars represent SEM ($n = 7$ technical replicates in primary tumor samples; $n = 5$ in metastatic samples). HR, hazard ratio.

an additional TMA containing 39 human high-grade HER2+ ductal breast cancer samples obtained before any treatment (TMA 2 in *Materials and Methods*). High HER2–CB_2R heteromer expression was also associated with poor patient prognosis, specifically lower disease-free and overall patient survival (Fig. 1 *C* and *D*). Positive and negative controls for HER2–CB_2R heteromer expression are shown in *SI Appendix*, Fig. S1 *A–D*. The separate analysis of either HER2 or CB_2R by immunohistochemistry confirmed two issues. First is that increased heteromer expression is not just a consequence of individual receptor overexpression. Thus, similar HER2–CB_2R heteromer levels were found in tumors with low, medium, or high HER2 expression (*SI Appendix*, Fig. S1*E*), as well as with no, low, medium, or high CB_2R expression (*SI Appendix*, Fig. S1*F*). Second is that HER2–CB_2R heteromer expression is a better prognostic marker than HER2 alone or CB_2R alone. Thus, no association between HER2 expression and disease-free survival was found in TMA 1 (*SI Appendix*, Fig. S2*A*); for CB_2R expression, although there seemed to be an association trend with disease-free survival, it did not reach statistical significance either (*SI Appendix*, Fig. S2*B*). In addition, we analyzed heteromer expression in two pairs of patient-derived xenografts (PDXs). Each pair consisted of one PDX generated from the patient's primary tumor and another PDX generated from the corresponding metastasis (in the liver in one case, and in a lymph node in the other). Consistent with the idea that HER2–CB_2R complexes correlate with poor patient prognosis, in both cases we observed significantly higher heteromer expression in the metastatic tissue with respect to the corresponding primary tumor (Fig. 1 *E* and *F*). Together, these results show that HER2–CB_2R heteromers are specific receptor complexes present in HER2+ breast cancer tissue, and are associated with tumor recurrence and spreading.

Δ^9-Tetrahydrocannabinol Disrupts HER2–CB_2R Complexes and Impairs HER2+ Breast Cancer Cell Viability. Since HER2–CB_2R heteromer expression seems to be linked to prooncogenic processes (12) (Fig. 1), we next studied whether these complexes could be targets for antitumor therapies. It has been previously described that CB_2R activation in different models of HER2+ breast cancer leads to cancer cell death by apoptosis and inhibition of tumor growth, angiogenesis, and metastasis (10, 11). To determine if HER2–CB_2R heteromers are involved in this cannabinoid antitumor action, we analyzed their expression in response to Δ^9-tetrahydrocannabinol (THC; the main bioactive constituent of cannabis). We first used HEK293 cells transiently transfected with HER2 and CB_2R as a model. In this system, we confirmed the formation of HER2–CB_2R complexes by bioluminescence resonance energy transfer (BRET) (Fig. 2 *A* and *B*). The heteromer signal significantly decreased upon THC treatment (Fig. 2*C*). The cannabinoid-induced decrease in both HER2–CB_2R and cell viability relied on CB_2R activation, as indicated by the preventive effect of the CB_2R-selective antagonist SR144528 (SR2; Fig. 2 *C* and *E*). In addition, and supporting the idea that HER2–CB_2R heteromers are unique signaling structures, we observed that upon exposure to THC, CB_2R coupling shifts to a different set of heterotrimeric G proteins. Thus, in cells only expressing CB_2R, THC induced the coupling of the receptor to $G_{q/11}$, while it promoted the coupling to G_i and G_z when HER2 and CB_2R were coexpressed (*SI Appendix*, Fig. S3).

To determine whether the effects observed in HEK293 cells also occur in more physiological settings, we ran a series of experiments in two different human HER2+ breast cancer cell lines (BT474 and HCC1954). THC decreased the viability of both cell lines in a concentration-dependent manner (Fig. 2*F*), an effect that was again prevented by SR2 (Fig. 2*G*). The interaction between HER2 and CB_2R in these cells was then analyzed by coimmunoprecipitation upon overexpression of an HA-tagged form of CB_2R. THC treatment diminished the amount of CB_2R that coimmunoprecipitated with HER2 in both cell lines, which points to a cannabinoid-induced disruption of the heteromer (Fig. 2*H*). The decrease in HER2–CB_2R complexes was not due to a reduction in the receptors' expression, as they remained unchanged after a 4-h THC treatment (Fig. 2*H*). To further support the idea that THC disrupts HER2–CB_2R heteromers, we performed PLAs in the two breast cancer cell lines in native conditions (i.e., under no overexpression of HER2 or CB_2R). Data showed that THC decreases the amount of these complexes by activating CB_2R (Fig. 2 *I* and *J*).

HER2–CB_2R Heteromer Disruption by THC Hampers HER2 Activation. HER2 activation occurs upon dimerization with other members of the HER family, followed by *trans*- and autophosphorylation of the intracellular domains of each protomer (13). We analyzed whether disruption of the HER2–CB_2R heteromer by THC had any effect on this activation process. First, and to determine which specific HER dimers may be affected by HER2–CB_2R disruption, we evaluated the expression of the four members of the HER family in the two HER2+ cell lines used in our studies. In addition to HER2, we found HER1 and HER3 overexpression in at least one of them compared with a luminal (MCF7) or a basal (MDA-MB-231) breast cancer cell line (Fig. 3*A*). We therefore studied the effect of THC on HER2–HER1, HER2–HER2, and HER2–HER3 heteromers in HCC1954 cells. Neither HER2–HER1 nor HER2–HER3 complexes were affected by cannabinoid treatment (Fig. 3 *B* and *C*). In contrast, THC significantly diminished the amount of HER2–HER2 homodimers (Fig. 3 *B* and *C*), and this effect was prevented by SR2 (Fig. 3 *D* and *E*). HER2–HER2 homodimer reduction upon THC challenge, and involvement of CB_2R in this effect, were further confirmed by BRET in HEK293 HER2–CB_2R cells (Fig. 3*F*). As expected, THC produced no such action in HEK293 cells lacking CB_2 receptors (Fig. 3*G*). In line with these observations, THC decreased the levels of HER2 phosphorylated at Tyr1248 (Fig. 3 *H* and *I*), one of the main autophosphorylation sites in this receptor. Taken together, these observations demonstrate that HER2–CB_2R heteromer disruption by THC hampers HER2 activation by interfering with its homodimerization.

THC Induces HER2–CB_2R Heteromer Disruption and HER2 Degradation in Vitro and in Vivo. Cannabinoid challenge produced a marked decrease in the levels of activated (phospho-Tyr1248) HER2 (Figs. 3 *H* and *I* and 4 *A* and *B*), that was followed by a decrease in the total levels of HER2 (Fig. 4 *A* and *B*). This effect was prevented by blockade of CB_2R (Fig. 4*C*), and was not due to inhibition of gene transcription, as indicated by the observation that HER2 mRNA levels remained unchanged (Fig. 4*D*). These results suggest that THC produces both an impairment of HER2 prooncogenic activity and the triggering of antitumoral signaling through CB_2R activation. In line with this notion, inactivation of both ERK and AKT was observed 24 h after THC treatment, and this was prevented by CB_2R pharmacological blockade as well as by HER2 knockdown, which reduced pERK and pAKT per se (*SI Appendix*, Fig. S4).

Importantly, THC also produced the disruption of HER2–CB_2R heteromers in vivo, an effect that was associated with HER2 degradation and antitumor responses. Thus, THC significantly decreased the growth of orthotopic xenografts generated in immunodeficient mice by injection of HCC1954 cells (Fig. 4*E*), and tumors from the THC-treated group showed significantly reduced HER2 protein levels (Fig. 4 *F* and *G*) as well as significantly reduced HER2–CB_2R and HER2–HER2 PLA signal (Fig. 4 *H* and *I*), compared with vehicle-treated animals.

One of the main mechanisms of intracellular protein degradation is proteolytic hydrolysis by the proteasome (14). Blockade of the proteasome system with lactacystin prevented the decrease of HER2 levels induced by THC in BT474 breast cancer cells (Fig. 5 *A* and *B*). We performed similar experiments in HCC1954 cells, but they showed hypersensitivity to proteasome inhibition and died in response to low concentrations of lactacystin. THC also increased the levels of ubiquitinated HER2 (Fig. 5*C*). The main E3 ligases reported so far to be responsible for HER2 degradation are CHIP and c-CBL (15). While cannabinoid treatment did not modify the levels of the former, it significantly

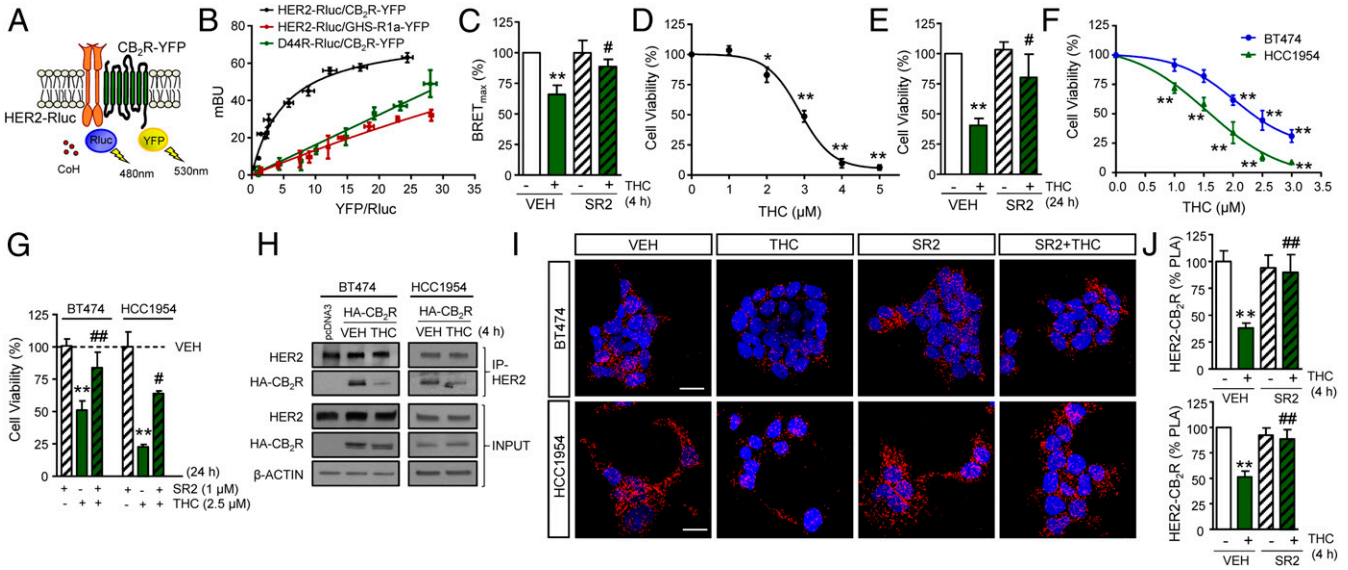

Fig. 2. THC decreases HER2–CB_2R complexes. (*A*) Schematic representation of bioluminescence resonance energy transfer experiments. (*B*) BRET saturation curve in HEK293 cells transfected with a fixed concentration of HER2-Rluc and increasing concentrations of CB_2R-YFP. HER2-Rluc/GHS-R1a-YFP and D44R-Rluc/YFP were used as negative controls for the interaction ($n = 8$). (*C*) Effect of THC (4 h), alone or in combination with the CB_2R-selective antagonist SR144528 (SR2; 1 μM), on HER2-Rluc/CB_2R-YFP $BRET_{max}$ signal in HEK293 cells ($n = 3$). (*D* and *E*) Viability of CB_2R- and HER2-transfected HEK293 cells after 24-h treatment with increasing concentrations of THC ($n = 5$) (*D*), or THC in combination with SR2 (1 μM) ($n = 4$) (*E*). (*F* and *G*) Viability of BT474 ($n = 6$) and HCC1954 ($n = 3$) cells in response to increasing concentrations of THC (*F*), or in combination with the CB_2R-selective antagonist SR144528 (1 μM) (*G*). Results ($n = 3$ to 6 independent experiments) are expressed as percent vs. vehicle-treated cells, set at 100%, and error bars represent SEM. (*H*) Coimmunoprecipitation of HER2 with CB_2R after THC treatment (4 h), in BT474 and HCC1954 cells transfected with an HA-tagged CB_2R plasmid. IP, immunoprecipitation. (*I*) Representative PLA confocal microscopy images of HER2–CB_2R heteromers (in red) in BT474 (*Upper*) and HCC1954 cells (*Lower*), treated with THC (4 h) alone or in combination with SR2 (1 μM). Cell nuclei are stained in blue. (Scale bars, 25 μm.) (*J*) Quantification of HER2–CB_2R PLA signal (number of red dots per cell) ($n = 3$). Results are expressed as percent vs. vehicle-treated cells, set at 100%, and error bars represent SEM. Multigroup comparisons were analyzed by one-way ANOVA with Tukey's post hoc test. $^{*}P < 0.05$, $^{**}P < 0.01$ vs. vehicle-treated cells; $^{\#}P < 0.05$, $^{\#\#}P < 0.01$ vs. THC.

increased the amount of c-CBL in BT474 and HCC1954 cells (Fig. 5 *D* and *E*). Moreover, THC augmented the extent of HER2 phosphorylation at Tyr1112, the residue that is specifically recognized by c-CBL and triggers HER2 polyubiquitination (16) (Fig. 5*F*). Involvement of c-CBL in HER2 degradation was further supported by genetic blockade. siRNA-driven targeting of this E3 ligase prevented THC-induced decrease of total HER2 levels in the two breast cancer cell lines tested (Fig. 5 *G* and *H*).

Collectively, these findings demonstrate that THC disrupts HER2–CB_2R heteromers, blocks HER2 activation, and promotes its degradation through the proteasome system via c-CBL activation, which results in antitumor responses.

HER2–CB_2R Heteromer Disruption by Targeting CB_2R Transmembrane 5 Mimics THC Effects. To determine whether the effects described above were THC-specific or could also be produced by other tools that disrupt HER2–CB_2R heteromers, we used two different experimental approaches aimed at blocking the physical interaction between HER2 and CB_2R. First, and to determine which part of the cannabinoid receptor is involved in the interaction with HER2, we generated a series of truncated proteins containing the N-terminal domain of CB_2R, followed by one of the seven transmembrane (TM) domains of the receptor and its C-terminal domain. All constructs contained an HA tag in the N-terminal domain (Fig. 6*A*). Coimmunoprecipitation assays in HEK293 cells cotransfected with HER2 and the different CB_2R constructs showed a potential interaction between HER2 and TMs 1, 3, 4, and 5 of CB_2R (Fig. 6*B*). To determine which of them was more plausible to participate in the physical interaction between the two receptors, we performed bimolecular fluorescence complementation (BiFC) assays in HEK293 cells (Fig. 6*C*). A fluorescent, proximity-evoked signal was observed when the HER2 fusion protein was cotransfected with the CB_2R fusion protein and the constructs containing CB_2R TMs 1, 2, 3, 6, and 7 (Fig. 6*D*). This signal was significantly reduced upon cotransfection with CB_2R TMs 4 and 5 (Fig. 6*D*), which is indicative of heteromer disruption. Since TM5 has been previously described to be involved in interactions between GPCRs (17–19), we focused our studies on this specific transmembrane domain. A TM5-targeted peptide (CB_2R TAT-TM5) was then used to prevent the association between CB_2R and HER2. The use of this type of peptide has been widely reported in the literature, and it is broadly accepted as a tool for disrupting GPCR–GPCR interaction (20, 21). BiFC experiments confirmed that this tool selectively blocks the formation of HER2–CB_2R heteromers (Fig. 6*E*). Thus, the fluorescent signal indicative of the presence of HER2–CB_2R heteromers disappeared when cells were incubated with the CB_2R TAT-TM5 peptide, and not when they were challenged with a D44R TAT-TM5–targeted peptide (used as negative control) (Fig. 6*E*). Similar data were obtained when PLAs were carried out in native untransfected HER2+ breast cancer cells (Fig. 7*A*), that is, a significant decrease in the dotted fluorescent signal corresponding to the heteromers appeared upon CB_2R TAT-TM5 treatment, which was not evident when the D44R TM5 peptide was used (Fig. 7 *A* and *B*). Of interest, and as observed for THC, disruption of HER2–CB_2R heteromers by the CB_2R TAT-TM5 peptide produced (*i*) HER2 inactivation, as demonstrated by a dramatic decrease in the formation of HER2–HER2 homodimers (Fig. 7 *C* and *D*) and in the levels of phosphorylated HER2 (Fig. 7 *E* and *F*); (*ii*) HER2 degradation, evidenced by a marked reduction in total HER2 protein levels (Fig. 7 *E* and *F*); and (*iii*) a concomitant decrease in the viability of HER2+ breast cancer cells (Fig. 7*G*) that was not observed in wild-type HEK293 cells, which do not express either HER2 or CB_2R (Fig. 7*G*). Altogether, these results show that disruption of HER2–CB_2R heteromers, either with THC or with other tools aimed at interfering with the physical interaction between CB_2R TM5 and the transmembrane domain of HER2, dramatically impairs the viability of HER2+ breast cancer cells.

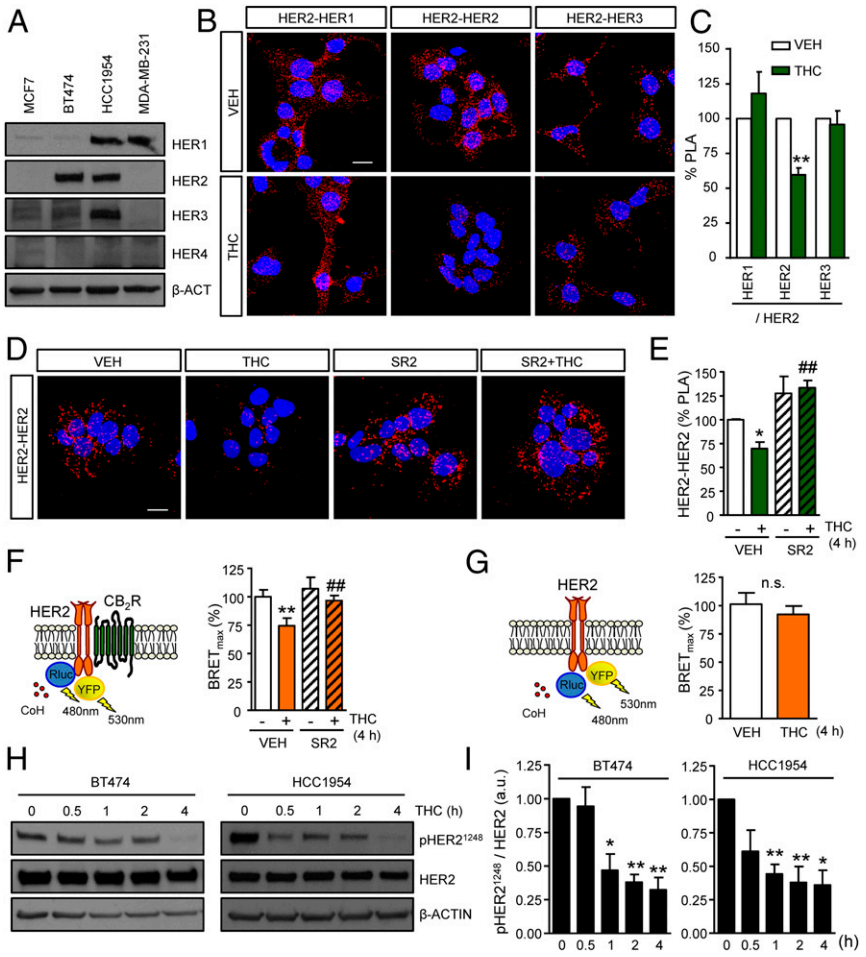

Fig. 3. HER2–CB_2R heteromer disruption by THC hampers HER2 activation. (*A*) HER1, HER2, HER3, and HER4 expression, as determined by Western blot analysis, in the indicated breast cancer cell lines. (*B*) Representative PLA confocal microscopy images of the effect of THC (4 h) on HER2–HER1 ($n = 4$), HER2–HER2 ($n = 5$), and HER2–HER3 ($n = 3$) dimers (in red) in HCC1954 cells (*B*), with the corresponding quantification (*C*), or on HER2–HER2 expression after THC treatment, alone or in combination with the CB_2R-selective antagonist SR144528 (1 μM) ($n = 3$) (*D*), with the corresponding quantification (*E*). Cell nuclei are in blue. (Scale bars, 20 μm.) (*F* and *G*, *Left*) Schematic representation of the BRET experiments conducted in HEK293 cells. CoH, coelenterazine H. (*F* and *G*, *Right*) Quantification of HER2-Rluc/HER2-YFP $BRET_{max}$ after THC treatment (4 h) alone or in combination with SR2 (1 μM) where indicated, in cells cotransfected with HER2-Rluc, HER2-YFP, and a CB_2R untagged receptor ($n = 3$) (*F*), or an empty vector ($n = 4$) (*G*) (used as a negative control for THC activation). In *C* and *E*–*G*, results are expressed as percent vs. vehicle-treated cells, set as 100%, and graph bars represent SEM. (*H*) Expression of $pHER2^{1248}$ in BT474 and HCC1954 cells, as determined by Western blot, upon THC treatment at the indicated times. (*I*) Quantification. Results are normalized vs. the corresponding total HER2 levels at each individual time point, and expressed as fold increase vs. time 0, set at 1 ($n = 4$ in BT474; $n = 7$ in HCC1954). Error bars represent SEM. Unpaired independent groups of two were analyzed by two-tailed Student's *t* test. When multigroup comparison was required, data were analyzed by one-way ANOVA with Tukey's post hoc test. $^{*}P < 0.05$, $^{**}P < 0.01$ vs. vehicle-treated cells; $^{\#\#}P < 0.01$ vs. THC. n.s., not significant.

Discussion

Here, we describe a mechanism controlling the activity of HER2 that may constitute a new target for antitumor treatments. Specifically, we observed that HER2 physically interacts with a membrane receptor that does not belong to the HER family (cannabinoid receptor CB_2R), thus forming HER2–CB_2R heteromers, and that disrupting these complexes triggers the inactivation and degradation of HER2, promoting in turn antitumoral responses. The HER2–CB_2R heteromers described herein fulfill the three criteria required for demonstrating receptor heteromerization (20, 21): First, the heteromer component (HER2 and CB_2R) interaction is demonstrated by proximity-based techniques and coimmunoprecipitation; second, HER2–CB_2R heteromers exhibit properties distinct from those of the protomers, as demonstrated by the coupling of CB_2R to different heterotrimeric G proteins depending on whether it is part of the heteromer or not; and third, heteromer disruption leads to a loss of heteromer-specific properties, as demonstrated by the fact that while HER2–CB_2R complexes are linked to prooncogenic events (12), disruption of the heteromers leads to antitumor responses.

Interaction of HER2 with other membrane receptor tyrosine kinases (RTKs) is a common and well-described process. Dimerization with other members of the HER family, for example, is a necessary step for HER activation, and in fact some drugs have been already designed to interfere with this step and block the subsequent prooncogenic signaling (4). An increasing number of studies demonstrate that GPCRs also interact physically between them, generating unique signaling platforms (GPCR heteromers) with physiopathological implications different from those of the constituting monomers. Most have been described in the central nervous system, and are becoming potential therapeutic targets for disorders such us addiction, pain, Parkinson's disease, and schizophrenia (21–23). Heteromers between cytokine and adrenergic receptors have also been described, with implications in blood pressure regulation (21, 23), or between different GPCRs in distinct endocrine systems, which may constitute new targets for endocrine-related disorders (24). Cannabinoid receptors in particular have been long described as constituents of particular GPCR receptor heteromers. Thus, CB_1R physically interacts with CB_2R (25), serotonin (26), adenosine (22, 27), opioid (28), orexin (29), and angiotensin (30) receptors, and with the cannabinoid-related orphan receptor GPR55 (31). CB_2R, on the other hand, has been shown to form heteromers with GPR55 (32, 33) and CXCR4 (34, 35). Although several RTK–RTK heteromers and GPCR–GPCR heteromers have been previously described, there are very few examples of physical interaction between RTKs and GPCRs yet. Transactivation of RTKs by GPCRs and vice versa has been reported and in some cases physical interactions have been suggested, but no solid proof of the existence of such heteromers has been provided in most cases (36). Usually, colocalization, coimmunoprecipitation, and pharmacological transmodulation of the protomers in nonnative cell systems are the only evidence suggesting the presence of the heteromer, but this is clearly insufficient. Colocalization does not provide enough subcellular resolution to establish close proximity, and even coimmunoprecipitation can occur with receptors too far apart to directly modulate one another. Transactivation is no doubt a very interesting pharmacological process, but demonstrating the existence of receptor heteromers has additional importance in terms of providing new druggable therapeutic targets. To the best of our knowledge, the best-characterized RTK–GPCR heteromer is that formed by HER2 and β_2-adrenergic

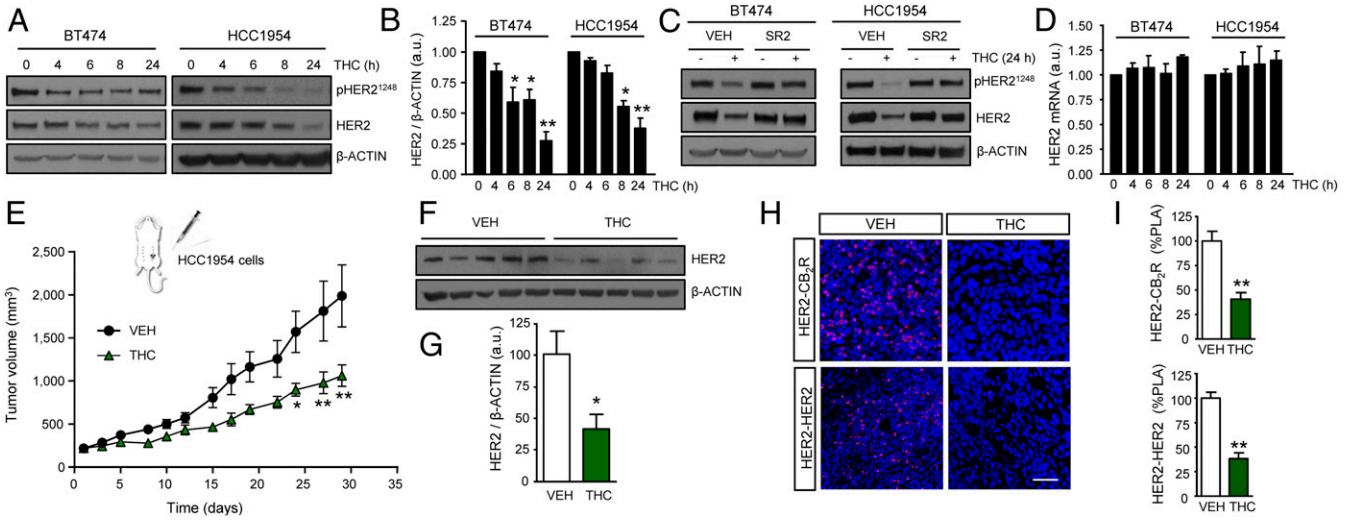

Fig. 4. HER2–CB_2R heteromer disruption by THC induces HER2 degradation in vitro and in vivo. (*A*, *B*, and *D*) Effect of THC on HER2 protein (*A* and *B*) and mRNA levels (*D*) at the indicated times, as determined by Western blot and qPCR, respectively, in BT474 and HCC1954 cells. For quantification, HER2 expression was normalized with the loading control [β-actin in *B*; β-actin and β-glucuronidase in *D*], and results ($n = 4$ in *B*; $n = 3$ in *D*) are expressed as fold increase vs. time 0, set at 1. Data were analyzed by one-way ANOVA. (*C*) Western blot analysis of the effect of the CB_2R-selective antagonist SR144528 (1 μM) on THC-induced HER2 protein decrease ($n = 4$ in BT474; $n = 7$ in HCC1954). (*E*) Growth of orthotopic tumors generated in NOD-SCID mice by injection of HCC1954 cells into the mammary fat pad. Animals were treated with vehicle (sesame oil) ($n = 10$) or THC (1.5 mg per dose) ($n = 9$) thrice a week. Results were analyzed by two-way ANOVA. (*F*) Representative Western blot of HER2 in the animal tumor samples. (G) Corresponding quantification. (*H*) Representative PLA confocal microscopy images of HER2–CB_2R and HER2–HER2 heteromers (red signal). Cell nuclei are in blue. (Scale bar, 50 μm.) (*I*) Quantification. Error bars in *B*, *D*, *E*, and *I* represent SEM. Unpaired, two-tailed Student's *t* test. $*P < 0.05$, $**P < 0.01$ vs. time 0 (*B*) or vehicle-treated animals in *E*, *G*, and *I*.

receptors in the heart, which seems to be essential for cardiac homeostasis (37); by fibroblast growth factor receptor and adenosine A_{2A} receptors (38) or serotonin 5-HT_{1A} receptors (39), which play important roles in synaptic plasticity; and by EGFR and GPR54, which seem to promote breast cancer cell invasiveness (40). Here, we comprehensively describe the existence of heteromers between HER2 and CB_2R and provide compelling evidence showing that their disruption promotes antitumoral responses both in vitro and in vivo, which may constitute a new strategy to treat HER2+ breast tumors. It is tempting to speculate that other HER2-overexpressing tumors such as gastric or gastroesophageal adenocarcinomas (41) may express similar CB_2R–HER2 heteromers, and therefore respond in a similar way to treatments aimed at breaking up these complexes.

Our previous work had shown that, in the absence of exogenously applied cannabinoids, CB_2R plays a protumoral role in HER2+ contexts (12). In line with that study, here we report that heteromer expression correlates with poor patient prognosis. On the other hand, there is solid evidence that pharmacological activation of CB_2R produces antitumoral responses in HER2+ preclinical settings (10, 11). Considering all these observations, we propose the following model for HER2–CB_2R function in breast cancer (Fig. 8). Under no pharmacological treatment, HER2+ breast cancer cells express high levels of HER2, which up-regulate the expression of CB_2R via the mechanisms described in ref. 12. HER2 and CB_2R then form heteromers in the plasma membrane, thereby protecting HER2 from degradation and favoring its canonical oncogenic signaling, resulting in protumoral responses (Fig. 8*A*). When cells are exposed to THC (or to other tools that prevent HER2–CB_2R interaction), the two receptors physically separate. In addition, HER2–CB_2R disruption triggers inactivation of HER2 (by breaking HER2–HER2 homodimers) and increases its susceptibility to degradation. As a final consequence of HER2 degradation and CB_2R activation, an antitumor response is produced (Fig. 8*B*). It is also conceivable that in cellular contexts of very high HER2 expression, the role of CB_2R in HER2 signaling may be less relevant than in those with just high HER2 levels. The experiments we have conducted clearly show a direct impact of THC on the viability of cancer cells in culture and also in vivo. However, we cannot rule out the involvement of other cell types in the full antitumor response induced by THC. For example, immune cells and endothelial cells express CB_2R as well, and it is reasonable to speculate that they may be affected by THC. In fact, it has been previously demonstrated, for example, that THC impairs tumor angiogenesis by blocking endothelial cell migration and blood vessel formation and elongation (reviewed in ref. 42). Of note, antitumor responses upon CB_2R activation have also been described in non-HER2+ contexts. It would be interesting to analyze whether in those situations CB_2R acts as a monomer in the plasma membrane or if it forms heteromers with other RTKs like HER1 (EGFR), which is overexpressed in many different types of tumors (41). In favor of the latter, Elbaz et al. (43) recently reported that CB_2R impairs oncogenic EGF/EGFR signaling in ER+ breast cancer cells. Although not proved, the authors suggested that EGFR and CB_2R may be forming complexes, and that CB_2R activation might disrupt them (43). In addition, and similar to what we observed here, pharmacological activation of CB_1R induced the death of prostate cancer cells in culture, an effect that was accompanied by a significant down-regulation of EGFR (44), and coexpression of EGFR with CB_1R was associated with poor patient prognosis in this type of cancer (45). These observations demonstrate a functional interaction between another cannabinoid receptor (CB_1R) and another member of the HER family (HER1) that could be due to a mere transactivation process or to a physical interaction similar to that described here between CB_2R and HER2.

In summary, our findings unveil a mechanism of regulation of HER2 activity, and support HER2–CB_2R heteromers as new therapeutic targets for the management of HER2+ breast cancer. Although THC efficiently achieves heteromer disruption, our data set the basis for the design of new antitumor drugs aimed at breaking this interaction. In addition, it would be interesting to design an alternative method to detect and quantify these heteromers in human samples. Thus, anti–HER2–CB_2R antibodies or similar tools would allow not only corroboration of the prognostic value described herein but also an easy transfer of this knowledge to clinical practice.

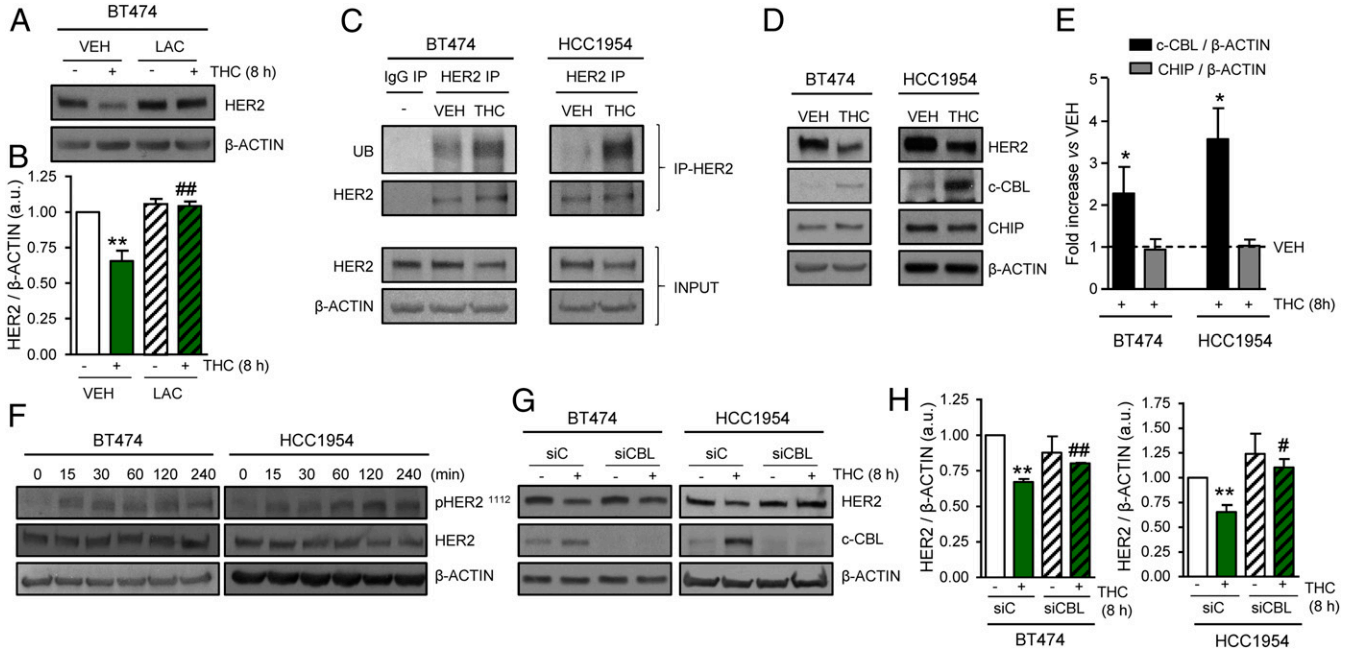

Fig. 5. HER2–CB_2R heteromer disruption by THC induces HER2 degradation via the c-CBL E3 ligase. Western blot-based analyses of the effect of different pharmacological and genetic tools on THC-induced HER2 degradation. (*A* and *B*) Effect of lactacystin (LAC; 1 μM) on BT474 cells ($n = 4$). (*C*–*F*) Effect of THC (4 h) on ubiquitinated HER2 (UB) (*C*), on c-CBL and CHIP levels (*D* and *E*), or on HER2 phosphorylation at Tyr1112 (*F*) in the indicated breast cancer cell lines. (*G* and *H*) HER2 protein expression after genetic silencing of c-CBL with selective siRNAs (siCBL). A nontargeted siRNA was used as a control (siC). The densitometric analyses of HER2 immunoblots were normalized to β-actin ($n = 4$ in *B*; $n = 6$ in *E*; $n = 4$ in *H*). Results are expressed as fold increase vs. vehicle-treated cells, set at 1, and graph bars represent SEM. Unpaired, independent groups of two were analyzed by two-tailed Student's *t* test. When multigroup comparison was required, data were analyzed by one-way ANOVA with Tukey's post hoc test. $^{*}P < 0.05$, $^{**}P < 0.01$ vs. vehicle-treated group; $^{\#}P < 0.05$, $^{\#\#}P < 0.01$ vs. THC-treated group.

Materials and Methods

Cell-Viability Assays. Cells were seeded at a density of 5,000/cm^2 in 10% FBS-containing medium. Twenty-four hours later, they were serum-starved overnight and then treated with THC for 24 h. Cells were then fixed and stained with a crystal violet solution (0.1% crystal violet, 20% methanol in H_2O) for 20 min. After intensive washing with water, the stained cells were solubilized in methanol and absorbance was measured at 570 nm.

Cell Cultures and Transfections. Human breast adenocarcinoma cell lines HCC1954 (CRL-2338), BT474 (HTB-20), MCF7 (HTB-22), and MDA-MB-231 (HTB-26) and the human embryonic kidney cell line HEK293T (CRL-1573) were purchased from American Type Culture Collection. They were all authenticated by short tandem repeat profiling (Genomics Core Facility at "Alberto Sols" Biomedical Research Institute) and routinely tested for mycoplasma contamination. Cells were cultured in RPMI (HCC1954, BT474), MEM (MCF7), or DMEM (MDA-MB-231, HEK293T) supplemented with 10% FBS and 1% penicillin/streptomycin, and BT474 and MCF7 cells with 10 μg/mL insulin as well. They were all maintained at 37 °C in an atmosphere of 5% CO_2.

For cell-culture experiments, THC (THC Pharm) was dissolved in DMSO. Unless otherwise indicated, the concentration used was 3 μM for HCC1954 cells and 4 μM for BT474 and HEK293T cells. The CB_2R-selective antagonist SR144528 (SR2) (Tocris Bioscience) and lactacystin (Calbiochem) were dissolved in DMSO and added to the cell cultures (1 μM) 1 h prior to THC.

Expression vectors were transiently transfected with FuGENE HD transfection reagent (Promega) in human breast cancer cells, and polyethylenimine (PEI) (Sigma-Aldrich) in HEK293T cells. Transient genetic knockdown was done by selective siRNA transfection with DharmaFECT 1 transfection reagent (Dharmacon). Selective siRNAs to knock down human c-CBL were purchased from Dharmacon as a SMARTpool. These reagents combine four SMART selection-designed siRNAs into a single pool, which guarantees an efficiency of silencing of at least 75%. Sequences were 5′-AAUCAACUCUGAACGAAA-3′, 5′-GACAAUCCUCACAAUAAA-3′, 5′-UAGCCCACCUUAUAUCUUA-3′, and 5′-GGAGACAUUUCGGAUUA-3′. The control (nontargeted) siRNA was purchased from Thermo Fisher Scientific.

Western Blot Analysis. Cells and tumors were lysed in RIPA buffer supplemented with 1 mM sodium orthovanadate, 1 mM PMSF, 2 μg/μL aprotinin, and 2 μg/μL leupeptin (Sigma-Aldrich). Total lysates were resolved by SDS/PAGE and electrophoretically transferred to PVDF membranes. After blocking with 5% (wt/vol) nonfat dry milk in TBS-Tween, membranes were incubated with the following antibodies overnight at 4 °C: rabbit polyclonal anti-HER2 (C-18; Santa Cruz Biotechnology); mouse monoclonal anti-HER2 (44E7) and rabbit polyclonal anti–phospho-HER2 (Tyr1248) (2247) (Cell Signaling Technology); rabbit polyclonal anti-HER1 (06-847; EMD Millipore); rabbit polyclonal anti-HER3 (1B2E, 4754; Cell Signaling Technology); rabbit polyclonal anti-HER4 (C-18; Santa Cruz Biotechnology); rabbit polyclonal anti-HA tag (C29F4; Cell Signaling Technology); mouse monoclonal anti–β-actin (AC-74; Sigma-Aldrich); mouse monoclonal anti–c-CBL (clone 17; BD Biosciences); mouse monoclonal anti-STUB1 (CHIP) (ab2917; Abcam); and mouse monoclonal anti-ubiquitin (P4D1; Santa Cruz Biotechnology). Secondary antibodies were chosen according to the species of origin of the primary antibodies, and detected by an enhanced chemiluminescence system (Bio-Rad). β-Actin was used as loading control. Densitometric analysis of the relative expression of the protein of interest vs. the corresponding control (β-actin or total HER2) was performed with ImageJ software (NIH).

Coimmunoprecipitation Assays. HCC1954 and BT474 cells were transiently transfected with pcDNA3.1-HA-hCB_2R (UMR cDNA Resource Center, University of Missouri, Rolla) or the corresponding empty vector (pcDNA3) (Invitrogen) with FuGENE HD transfection reagent (Promega). HEK293 cells were transiently cotransfected with pcDNA3-HER2, pcDNA3.1-HA-hCB_2R, or pcDNA3 containing the different CB_2R transmembrane constructs (see below) using PEI (Sigma-Aldrich). Forty-eight hours after transfection, cells were lysed in a buffer containing 40 mM Hepes (pH 7.5), 120 mM NaCl, 1 mM EDTA, 10 mM sodium pyrophosphate, 10 mM sodium glycerophosphate, 50 mM sodium fluoride, 0.5 mM sodium orthovanadate, and 0.3% CHAPS and supplemented with 1 mM benzamidine and 0.1 mM PMSF. Cell lysates (1 mg) were incubated with anti-HER2 antibody (C-18; Santa Cruz Biotechnology) covalently coupled to protein G-Sepharose (GE Healthcare) overnight at 4 °C on a rotating wheel. Immunoprecipitates were washed with lysis buffer and Hepes buffer (25 mM Hepes, pH 7.5, 50 mM KCl), resuspended in sample buffer, and filtered through a 0.22-μm pore size Spin-X filter (Sigma-Aldrich). 2-Mercaptoethanol was then added to a concentration of 1% (vol/vol), and samples were resolved by SDS/PAGE and transferred

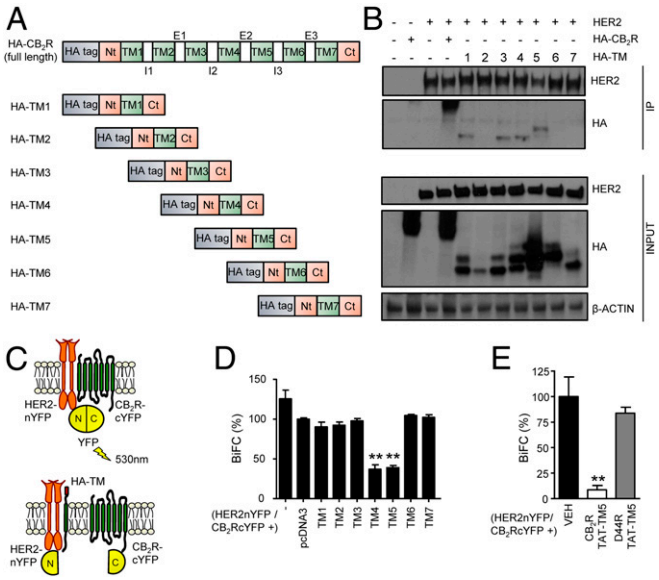

Fig. 6. CB_2R transmembrane domain 5 is involved in HER2–CB_2R heterodimerization. (*A*) Schematic representation of the HA-tagged truncated forms of CB_2R used in this study. Each construct contains the HA tag, followed by the N-terminal domain of the receptor, one of its seven transmembrane domains, and the C-terminal end. (*B*) Each of the seven CB_2R constructs (named HA-TMX, where X is the corresponding transmembrane domain) and a pcDNA3-HER2 plasmid was coexpressed in HEK293 cells. Immunoprecipitation of HER2 with an anti-HER2 antibody was followed by Western blot analysis with an anti-HA antibody. Full-length pcDNA3-HA-CB_2R was also coexpressed with HER2 as a positive control of interaction. (*C*) Schematic representation of the bimolecular fluorescence complementation experiments between HER2-cYFP and CB_2R-nYFP in the absence (*Upper*) or presence of the CB_2R transmembrane constructs (*Lower*). (*D* and *E*) Complementation signal (i.e., fluorescence at 530 nm) of HEK293 cells transfected with CB_2R-cYFP, HER2-nYFP, and the indicated CB_2R TM constructs ($n = 3$) (*D*), or after 4 h of incubation with the indicated TAT-TM peptides (4 μM) ($n = 3$) (*E*). Results were analyzed by one-way ANOVA with Tukey's post hoc test. Error bars represent SEM. $^{**}P < 0.01$ vs. pcDNA3 (*D*) or vehicle-treated group (*E*).

to PVDF membranes. Membranes were blotted with anti-HA antibody (Cell Signaling Technology).

Ubiquitination Assays. Cells were lysed after 4 h of THC or DMSO treatment using RIPA buffer supplemented with 1 mM sodium orthovanadate, 0.1 mM PMSF, and 20 mM *N*-ethylmaleimide. Cell lysates (1 mg) were immunoprecipitated with an anti-HER2 antibody (C-18; Santa Cruz Biotechnology) or preimmune IgG overnight at 4 °C on a rotating wheel. Cell lysates were then incubated with protein G-Sepharose and then washed in RIPA lysis buffer. Finally, immunoprecipitates were resuspended in sample buffer containing 2-mercaptoethanol. Samples were then resolved and electrophoretically transferred to PVDF membranes and blotted with mouse monoclonal anti-ubiquitin antibody (P4D1; Santa Cruz Biotechnology).

Real-Time Quantitative PCR. RNA was isolated with TRIzol reagent (Invitrogen), and cDNA was obtained with Transcriptor Reverse Transcriptase (Roche Applied Science). Real-time quantitative PCR assays were performed using FastStart Master Mix with Rox (Roche). The primers used for ERBB2 (HER2) were as follows: forward, 5′-GGGAAACCTGGAACTCACCT-3′; reverse, 5′-CCCTGCACCTCCTGGATA-3′. Each value was adjusted by using β-actin (forward, 5′-CCAACCGCGAGAAGATGA-3′; reverse, 5′-CCAGAGGCGTACAGGGATAG-3′) and β-glucuronidase (forward, 5′-CGCCCTGCCTATCTGTATTC-3′; reverse, 5′-TCCCCACAGGGAGTGTGTAG-3′) levels as references.

Immunohistochemistry. Tissue sections were subjected to a heat-induced antigen retrieval step before exposure to a rabbit polyclonal anti-CB_2R (101550; Cayman Chemical) or a rabbit anti-HER2 primary antibody (HercepTest; DAKO). Immunodetection was performed using the Envision method with diaminobenzidine as the chromogen (DAKO). To quantify CB_2R expression in the TMA, cases were scored as 0 (no staining), 1 (weak staining), 2 (moderate staining), or 3 (high staining). HER2 staining was scored in accordance with the HercepTest manufacturer's guidelines.

In Situ Proximity Ligation Assays. For PLAs in the TMA and in sections of the patient-derived xenografts, samples were deparaffinized and submitted to heat-induced antigen retrieval in sodium citrate buffer (10 mM sodium citrate, 0.05% Tween 20, pH 6.0). TMA-, PDX-, and xenograft-derived slices were permeabilized with PBS containing 0.01% Triton X-100. For PLAs in cell cultures, cells were seeded on glass coverslips at 5,000/cm^2. After overnight serum starvation, cells were treated for 4 h with THC, TAT-TM peptides (4 μM), or the corresponding vehicle. They were then fixed in 4% paraformaldehyde and permeabilized with 0.05% Triton X-100.

Heteromers were detected by using the Duolink In Situ PLA Detection Kit (Sigma-Aldrich) following the manufacturer's instructions. For detection of HER2–CB_2R heteromers, cells were incubated with equal amounts of a rabbit

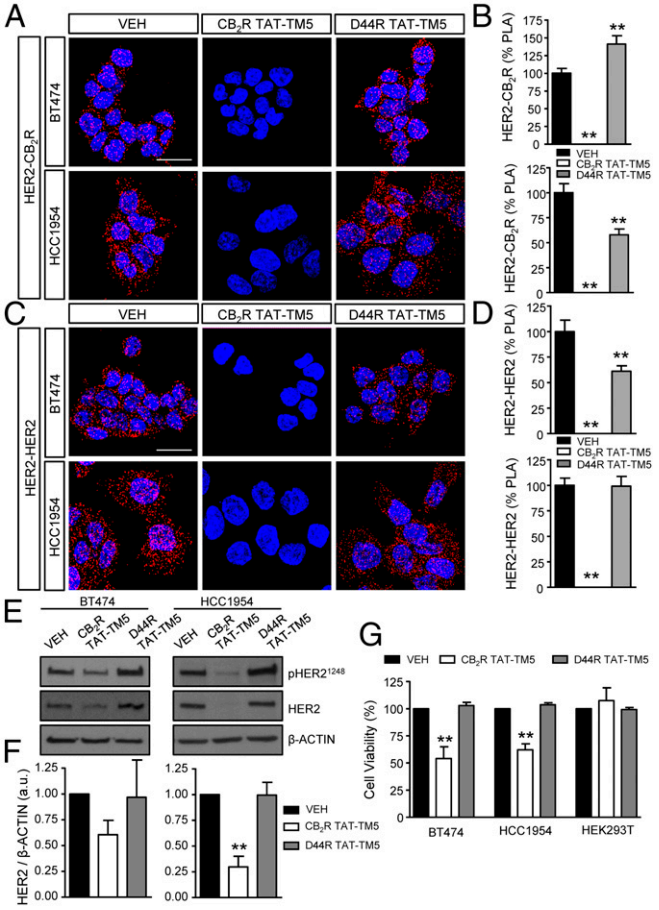

Fig. 7. HER2–CB_2R heteromer disruption by targeting CB_2R TM5 mimics THC effects. (*A–D*) Effect of TM peptides on HER2–CB_2R and HER2–HER2 heteromer expression as determined by PLA. (*A* and *C*) Representative PLA images in the indicated breast cancer cell lines, after treatment for 4 h with vehicle (DMSO), a TAT-TM peptide targeting CB_2R TM5 (4 μM), or a TAT-TM peptide targeting dopamine receptor D44 TM5 (4 μM), used as a negative control. Dimer signal is in red, and cell nuclei are in blue. (Scale bars, 25 μm.) (*B* and *D*) Results ($n =$ 7 technical replicates) are expressed as percent of PLA (red dots per cell) vs. vehicle-treated cells, set as 100%. (*E*) $pHER2^{1248}$ and HER2 protein levels, as determined by Western blot, after treatment with vehicle, CB_2R TAT-TM5, or D44R TAT-TM5 peptides for 24 h in BT474 and HCC1954 cells. (*F*) Densitometric analysis of HER2 normalized to β-actin ($n = 3$). Results are represented as fold increase vs. vehicle-treated cells, set as 1. (*G*) Viability of HCC1954, BT474, and HEK293 cells in response to the indicated treatments for 24 h. Data ($n = 4$) are represented as percent vs. vehicle-treated cells, set as 100%, and graph bars represent SEM. One-way ANOVA with Tukey's post hoc test. $^{**}P < 0.01$ vs. vehicle-treated cells.

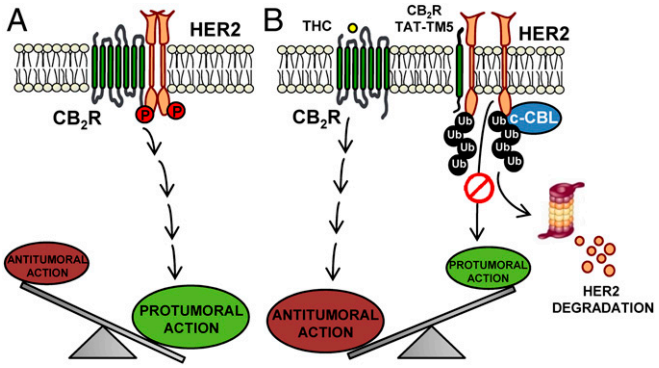

Fig. 8. Schematic drawing of the proposed mechanism of control of HER2 activity by CB_2R. (*A*) HER2 forms heteromers with CB_2R at the plasma membrane of HER2+ breast cancer cells, protecting it from degradation and favoring its prooncogenic signaling. (*B*) Disruption of HER2–CB_2R heteromers, either by THC or by specific tools targeting CB_2R transmembrane domain 5, triggers inactivation of HER2 by inducing the separation of HER2–HER2 homodimers and increasing HER2 susceptibility to degradation by the E3 ligase c-CBL. HER2 degradation and CB_2R activation result in antitumor responses.

anti-CB_2R antibody (101550; Cayman Chemical) directly linked to a plus PLA probe, and a rabbit anti-HER2 antibody (C-18; Santa Cruz Biotechnology) directly linked to a minus PLA probe. For detection of other HER2 heteromers, cells were incubated with a mixture of equal amounts of a mouse anti-HER2 antibody (44E7; Cell Signaling Technology) and rabbit anti-HER1 antibody (06-847; EMD Millipore) for HER2–HER1 detection, or with a rabbit anti-HER3 antibody (1B2E; Cell Signaling Technology) for HER2–HER3 detection. A plus anti-rabbit PLA probe and a minus anti-mouse PLA probe were used. For negative controls, one of the primary antibodies was omitted. Ligation and amplification were done with In Situ Detection Reagent Red (Sigma-Aldrich), and slices were mounted in DAPI-containing mounting medium. Samples were analyzed with a Leica SP2 confocal microscope (Leica Microsystems) and processed with ImageJ software. Heteromer expression was calculated as the number of red fluorescent spots (indicating that receptors are within sufficient proximity)/total cells in the field. Representative images for each condition were prepared for figure presentation by applying brightness and contrast adjustments uniformly using Adobe Photoshop CS5.

Fusion Proteins for BRET and BiFC Assays. Sequences encoding amino acid residues 1 to 155 and 156 to 238 of YFP Venus protein were subcloned into the pcDNA3.1 vector to obtain YFP Venus hemitruncated proteins. The human cDNAs for HER2, cannabinoid (CB_2R), dopamine (D44R), and Ghrelin (GHS-R1a) receptors, cloned into pcDNA3.1, were amplified without their stop codons using sense and antisense primers harboring EcoRI and BamHI sites to clone CB_2R and GHS-R1a; XhoI and EcoRI to clone D44R; or NheI and XhoI to clone HER2. The amplified fragments were subcloned to be in-frame with restriction sites of p*RLuc*-N1 (PerkinElmer) or pEYFP-N1 (enhanced yellow variant of GFP; Clontech) vectors, to generate plasmids that express proteins fused to Rluc or YFP on the C-terminal end (HER2-Rluc, D44R-Rluc, HER2-YFP, CB_2R-YFP, or GHS-R1a-YFP). For BiFC experiments, the cDNA for HER2, CB_2R, and D44R were also subcloned into pcDNA3.1-nVenus or pcDNA3.1-cVenus to generate a plasmid that expresses the receptor fused to the hemitruncated nYFP Venus or hemitruncated cYFP Venus on the C-terminal end of the receptor (HER2-nVenus, D44-nVenus, or CB_2R-cVenus).

CB_2R Transmembrane Mutants. A pCDNA3-HA-CB_2R plasmid was used as template for the generation of seven mutants containing an HA tag, followed by the N-terminal domain, one transmembrane domain, and the C-terminal domain of CB_2R. To assure the correct orientation of the resulting peptides, in constructs containing even-numbered transmembrane domains, the sequences corresponding to the transmembrane domains were reversed. The primers used to generate these constructs are shown in *SI Appendix*, Table S2.

HIV TAT-TM Peptides. Peptides containing the amino acid sequence of CB_2R and D4R transmembrane domains 5 were used as heteromer-disrupting agents. To allow intracellular delivery and the correct membrane orientation, they were fused (at the C-terminal domain) to the cell-penetrating HIV TAT peptide. Their resulting TAT-TM peptides were TM5-TAT CB_2R: DYLLSWLLFIAFLFSGIIYTYGHVLWYGRKKRRQRRR and TM5-TAT D4R: YVVYSSVCSFFLPCPLMLLLYWATFYGRKKRRQRRR.

They were synthetized at the Peptide Synthesis Facility at University Pompeu Fabra.

Bioluminescence Resonance Energy Transfer Assays. HEK293 cells were transiently cotransfected with a constant amount of a cDNA encoding HER2 or D44R fused to Rluc protein (HER2-Rluc, D44R-Rluc) as BRET donor, and with increasing amounts of a cDNA of the other receptor fused to YFP (CB_2R-YFP, HER2-YFP, GHS-R1a-YFP) as BRET acceptor. For quantification of protein-YFP expression, fluorescence at 530 nm was analyzed in a FLUOstar Optima fluorimeter (BMG Labtech). Fluorescence of cells expressing the BRET donor only was subtracted from these measurements. BRET signal was analyzed 1 min after addition of the bioluminescent substrate coelenterazine H (5 μM; Molecular Probes) with a Mithras LB 940 (Labnet Biotecnica). To quantify protein-Rluc expression, luminescence was determined 10 min after addition of 5 μM coelenterazine H. The net BRET is defined as [(long-wavelength emission)/(short-wavelength emission)] − Cf, where Cf corresponds to [(long-wavelength emission)/(short-wavelength emission)] for the Rluc construct expressed alone in the same experiment. BRET is expressed as milli-BRET units (mBU; net BRET × 1,000). In BRET curves, BRET was expressed as a function of the ratio between fluorescence and luminescence × 100 (YFP/Rluc). To calculate maximum BRET ($BRET_{max}$) from saturation curves, data were fitted using a nonlinear regression equation and assuming a single phase with GraphPad Prism software.

Bimolecular Fluorescence Complementation Assays. HEK293 cells cotransfected with HER2 fused to the YFP Venus N terminus (nYFP) and CB_2R fused to the YFP Venus C terminus (cYFP) were treated with vehicle, the CB_2R mutants, or the indicated TAT-TM peptides (4 μM) for 4 h at 37 °C. Fluorescence at 530 nm (which only appears after YFP complementation due to proximity of the two receptors fused to cYFP and nYFP hemiproteins) was quantified in a FLUOstar Optima fluorimeter (BMG Labtech). Protein fluorescence expression was determined as the fluorescence of the sample minus fluorescence of nontransfected cells. Cells expressing HER2-nYFP and nYFP or CB_2R-cYFP and cYFP showed similar fluorescence levels to nontransfected cells.

Antibody-Capture [^{35}S]GTPγS Scintillation Proximity Assays. Specific activation of different subtypes of G_α proteins by THC (5 μM) was determined as previously described (46). Briefly, cell-membrane homogenates from the four different cell lines [HEK293 cells transiently overexpressing HER2, CB_2R, both receptors (HER2–CB_2R) simultaneously, or the corresponding empty vector (pcDNA3)] were incubated in 96-well Isoplates (PerkinElmer Life Sciences) in incubation buffer containing 0.4 nM [^{35}S]GTPγS (PerkinElmer) and 50 or 100 μM GDP for G_{i2}, $G_{q/11}$, and G_o, or for G_{i1},G_{i3}, G_z, G_s, and $G1_{2/13}$ proteins, respectively. Specific antibodies for each G_α subunit (mouse monoclonal anti-$G_{\alpha i}1$ and anti-$G_{\alpha o}$, and rabbit polyclonal anti-$G_{\alpha i2}$, anti-$G_{\alpha i3}$, anti-$G_{\alpha z}$, anti-$G_{\alpha q/11}$, anti-$G_{\alpha s}$, and anti-$G_{\alpha 12/13}$; Santa Cruz Biotechnologies) and PVT scintillation proximity assay beads coated with protein A (PerkinElmer) were used. Radioactivity was quantified on a MicroBeta TriLux scintillation counter (PerkinElmer).

Animals and Treatments. All procedures involving animals were performed with the approval of the Complutense University Animal Experimentation Committee and Madrid Regional Government, according to European official regulations. For the generation of orthotopic tumors, 5×10^6 HCC1954 cells were injected into the fourth right mammary fat pad of anesthetized (with 4% isoflurane) 6-wk-old SCID female mice (Envigo). Tumor volume was routinely measured with an external caliper, and when it reached an average volume of 200 mm^3, animals were randomly assigned to the different experimental groups: THC (1.5 $mg \cdot animal^{-1} \cdot dose^{-1}$) or sesame oil as vehicle. Treatments were administered orally by gavage in 100 μL, three times a week for 1 mo. At the end of the treatment, animals were killed and tumors and organs were collected. Tumors were divided into portions for preparation of tissue sections for PLA staining (frozen in Tissue-Tek) and protein extraction (snap-frozen), and were stored at −80 °C until analysis. For PLA experiments, tumor samples were fixed by immersion in 4% paraformaldehyde solution for 24 h at 4 °C, washed in PBS, and cryopreserved in a 30% sucrose solution at 4 °C. Before sectioning, tumors were frozen in Tissue-Tek, and 20-μm-thick slices were cut on a freezing cryostat (Leica Jung CM-3000) and mounted on glass slides.

Patient-Derived Xenografts. Human breast tumors used to establish PDXs were from biopsies or surgical resections at Vall d'Hebron University Hospital, and were obtained following the institutional guidelines and approval of

the institutional review boards at Vall d'Hebron University Hospital in accordance with the Declaration of Helsinki. Written informed consent was obtained from all patients who provided tissue. Fragments of patient samples were implanted into the mammary fat pad of NOD CB17-Prkdcscid (NOD/SCID) (SM-NOD-5S-F; Janvier) and maintained with 17β-estradiol (1 μM) (E8875-1G; Sigma) in the drinking water. Mice were maintained and treated in accordance with the institutional guidelines of the Vall d'Hebron University Hospital Care and Use Committee.

Tissue Microarrays. Two different tumor series, in a TMA format, were used in this study. TMA 1 consisted of 57 samples corresponding to newly diagnosed HER2+ breast cancer patients operated at 12 de Octubre University Hospital between 1999 and 2013, and prior to any treatment. TMA 2 was previously described in ref. 47, and contained 138 high-grade ductal breast cancer samples obtained before treatment at the Vall d'Hebron University Hospital, Virgen del Rocío Hospital (Seville, Spain), and MD Anderson Cancer Center (Madrid, Spain) between 2003 and 2014. Of them, 39 corresponded to HER2+ cases. In both cases, paraformaldehyde-fixed and paraffin-embedded blocks of tumor tissue were used to generate the corresponding TMAs by punching two 1-mm spots of each patient's biopsy.

Statistics. Kaplan–Meier survival curves were statistically compared by the log-rank test. The best cutoff was manually selected for each TMA. In TMA 1, the PLA signal ranged from 1.3 to 16.0, and the cutoff was set at 8.0. In TMA 2, the PLA signal ranged from 1.5 to 6.0, and the cutoff was set at 4.0. Unpaired, independent groups of two were analyzed by two-tailed Student's *t* test. When multigroup comparison was required, data were analyzed by one-way ANOVA with Tukey's post hoc test. Tumor growth curves from vehicle- and THC-treated animals were statistically compared by two-way ANOVA. Significance level was below 0.05 in all cases. Results are shown as mean ± SEM, and the number of experiments is indicated in every case. All analyses were carried out using GraphPad software.

Data supporting the findings of this study are available within the paper and *SI Appendix*.

ACKNOWLEDGMENTS. We are indebted to the members of our laboratories for critical discussion on this work, especially to Dr. de Salas-Quiroga, and to Eva Resel for administrative support. This work was supported by grants from the Spanish Ministry of Economy and Competitiveness [supported with European Regional Development funds: PI14/01101 and PI17/00041 (to C.S. and E.P.-G.), and PI16/00134 (to G.M.-B.); CIBERONC (CB16/12/00295, to G.M.-B.); Fundació La Marató TV3 (20140610, to E.I.C.); Fundación Asociación Española Contra el Cáncer (to E.P.-G.); Zelda Therapeutics (to C.S. and M.G.); and Fundación Mutua Madrileña (2013/0072, to L.M.)]. S.B.-B. and I.T. are recipients of a Formación de Profesorado Universitario and pFIS fellowship (from the Spanish Ministry of Economy and Competitiveness). P.J.M. would like to acknowledge funding from the Biotechnology and Biological Sciences Research Council (BBSRC) Doctoral Training Programme.

1. Baselga J, Coleman RE, Cortés J, Janni W (2017) Advances in the management of HER2-positive early breast cancer. *Crit Rev Oncol Hematol* 119:113–122.
2. Russnes HG, Lingjærde OC, Børresen-Dale AL, Caldas C (2017) Breast cancer molecular stratification: From intrinsic subtypes to integrative clusters. *Am J Pathol* 187:2152–2162.
3. Tebbutt N, Pedersen MW, Johns TG (2013) Targeting the ERBB family in cancer: Couples therapy. *Nat Rev Cancer* 13:663–673.
4. Arteaga CL, Engelman JA (2014) ERBB receptors: From oncogene discovery to basic science to mechanism-based cancer therapeutics. *Cancer Cell* 25:282–303.
5. Loibl S, Gianni L (2017) HER2-positive breast cancer. *Lancet* 389:2415–2429.
6. Caffarel MM, Andradas C, Pérez-Gómez E, Guzmán M, Sánchez C (2012) Cannabinoids: A new hope for breast cancer therapy? *Cancer Treat Rev* 38:911–918.
7. Velasco G, Sánchez C, Guzmán M (2012) Towards the use of cannabinoids as antitumour agents. *Nat Rev Cancer* 12:436–444.
8. Schwarz R, Ramer R, Hinz B (2018) Targeting the endocannabinoid system as a potential anticancer approach. *Drug Metab Rev* 50:26–53.
9. Blasco-Benito S, et al. (2018) Appraising the "entourage effect": Antitumor action of a pure cannabinoid versus a botanical drug preparation in preclinical models of breast cancer. *Biochem Pharmacol* 157:285–293.
10. Caffarel MM, et al. (2010) Cannabinoids reduce ErbB2-driven breast cancer progression through Akt inhibition. *Mol Cancer* 9:196.
11. Nasser MW, et al. (2011) Crosstalk between chemokine receptor CXCR4 and cannabinoid receptor CB2 in modulating breast cancer growth and invasion. *PLoS One* 6: e23901.
12. Pérez-Gómez E, et al. (2015) Role of cannabinoid receptor CB2 in HER2 pro-oncogenic signaling in breast cancer. *J Natl Cancer Inst* 107:djv077.
13. Lemmon MA, Schlessinger J (2010) Cell signaling by receptor tyrosine kinases. *Cell* 141:1117–1134.
14. Varshavsky A (2017) The ubiquitin system, autophagy, and regulated protein degradation. *Annu Rev Biochem* 86:123–128.
15. Ohta T, Fukuda M (2004) Ubiquitin and breast cancer. *Oncogene* 23:2079–2088.
16. Klapper LN, Waterman H, Sela M, Yarden Y (2000) Tumor-inhibitory antibodies to HER-2/ErbB-2 may act by recruiting c-Cbl and enhancing ubiquitination of HER-2. *Cancer Res* 60:3384–3388.
17. Borroto-Escuela DO, et al. (2010) Characterization of the A2AR-D2R interface: Focus on the role of the C-terminal tail and the transmembrane helices. *Biochem Biophys Res Commun* 402:801–807.
18. Franco R, Martínez-Pinilla E, Lanciego JL, Navarro G (2016) Basic pharmacological and structural evidence for class A G-protein-coupled receptor heteromerization. *Front Pharmacol* 7:76.
19. Gaitonde SA, González-Maeso J (2017) Contribution of heteromerization to G protein-coupled receptor function. *Curr Opin Pharmacol* 32:23–31.
20. Ferré S, et al. (2014) G protein-coupled receptor oligomerization revisited: Functional and pharmacological perspectives. *Pharmacol Rev* 66:413–434.
21. Gomes I, et al. (2016) G protein-coupled receptor heteromers. *Annu Rev Pharmacol Toxicol* 56:403–425.
22. Brugarolas M, et al. (2014) G-protein-coupled receptor heteromers as key players in the molecular architecture of the central nervous system. *CNS Neurosci Ther* 20: 703–709.
23. Guidolin D, Agnati LF, Marcoli M, Borroto-Escuela DO, Fuxe K (2015) G-protein-coupled receptor type A heteromers as an emerging therapeutic target. *Expert Opin Ther Targets* 19:265–283.
24. Jonas KC, Hanyaloglu AC (2017) Impact of G protein-coupled receptor heteromers in endocrine systems. *Mol Cell Endocrinol* 449:21–27.
25. Callén L, et al. (2012) Cannabinoid receptors CB1 and CB2 form functional heteromers in brain. *J Biol Chem* 287:20851–20865.
26. Viñals X, et al. (2015) Cognitive impairment induced by delta9-tetrahydrocannabinol occurs through heteromers between cannabinoid CB1 and serotonin 5-HT2A receptors. *PLoS Biol* 13:e1002194.
27. Moreno E, et al. (2018) Singular location and signaling profile of adenosine A_{2A}-cannabinoid CB_1 receptor heteromers in the dorsal striatum. *Neuropsychopharmacology* 43:964–977.
28. Bushlin I, Gupta A, Stockton SD, Jr, Miller LK, Devi LA (2012) Dimerization with cannabinoid receptors allosterically modulates delta opioid receptor activity during neuropathic pain. *PLoS One* 7:e49789.
29. Ward RJ, Pediani JD, Milligan G (2011) Heteromultimerization of cannabinoid CB(1) receptor and orexin OX(1) receptor generates a unique complex in which both protomers are regulated by orexin A. *J Biol Chem* 286:37414–37428.
30. Rozenfeld R, et al. (2011) AT1R-CB_1R heteromerization reveals a new mechanism for the pathogenic properties of angiotensin II. *EMBO J* 30:2350–2363.
31. Martínez-Pinilla E, et al. (2014) CB1 and GPR55 receptors are co-expressed and form heteromers in rat and monkey striatum. *Exp Neurol* 261:44–52.
32. Balenga NA, et al. (2014) Heteromerization of GPR55 and cannabinoid CB2 receptors modulates signalling. *Br J Pharmacol* 171:5387–5406.
33. Moreno E, et al. (2014) Targeting CB2-GPR55 receptor heteromers modulates cancer cell signaling. *J Biol Chem* 289:21960–21972.
34. Coke CJ, et al. (2016) Simultaneous activation of induced heterodimerization between CXCR4 chemokine receptor and cannabinoid receptor 2 (CB2) reveals a mechanism for regulation of tumor progression. *J Biol Chem* 291:9991–10005.
35. Scarlett KA, et al. (2018) Agonist-induced CXCR4 and CB2 heterodimerization inhibits Gα13/RhoA-mediated migration. *Mol Cancer Res* 16:728–739.
36. Pyne NJ, Pyne S (2011) Receptor tyrosine kinase-G-protein-coupled receptor signalling platforms: Out of the shadow? *Trends Pharmacol Sci* 32:443–450.
37. Negro A, et al. (2006) erbB2 is required for G protein-coupled receptor signaling in the heart. *Proc Natl Acad Sci USA* 103:15889–15893.
38. Flajolet M, et al. (2008) FGF acts as a co-transmitter through adenosine A(2A) receptor to regulate synaptic plasticity. *Nat Neurosci* 11:1402–1409.
39. Borroto-Escuela DO, et al. (2012) Fibroblast growth factor receptor 1–5-hydroxytryptamine 1A heteroreceptor complexes and their enhancement of hippocampal plasticity. *Biol Psychiatry* 71:84–91.
40. Zajac M, et al. (2011) GPR54 (KISS1R) transactivates EGFR to promote breast cancer cell invasiveness. *PLoS One* 6:e21599.
41. Mishra R, Hanker AB, Garrett JT (2017) Genomic alterations of ERBB receptors in cancer: Clinical implications. *Oncotarget* 8:114371–114392.
42. Ramer R, Hinz B (2016) Antitumorigenic targets of cannabinoids—Current status and implications. *Expert Opin Ther Targets* 20:1219–1235.
43. Elbaz M, Ahirwar D, Ravi J, Nasser MW, Ganju RK (2017) Novel role of cannabinoid receptor 2 in inhibiting EGF/EGFR and IGF-I/IGF-IR pathways in breast cancer. *Oncotarget* 8:29668–29678.
44. Mimeault M, Pommery N, Wattez N, Bailly C, Hénichart JP (2003) Anti-proliferative and apoptotic effects of anandamide in human prostatic cancer cell lines: Implication of epidermal growth factor receptor down-regulation and ceramide production. *Prostate* 56:1–12.
45. Fowler CJ, Hammarsten P, Bergh A (2010) Tumour cannabinoid CB(1) receptor and phosphorylated epidermal growth factor receptor expression are additive prognostic markers for prostate cancer. *PLoS One* 5:e15205.
46. Diez-Alarcia R, et al. (2016) Biased agonism of three different cannabinoid receptor agonists in mouse brain cortex. *Front Pharmacol* 7:415.
47. Hergueta-Redondo M, et al. (2016) Gasdermin B expression predicts poor clinical outcome in HER2-positive breast cancer. *Oncotarget* 7:56295–56308.